Supporting Information

Yang et al. 10.1073/pnas.0909589106

SI Methods

Integrin αIIbβ3 Transmembrane-Cytoplasmic (TMCD) Domain Expression and Purification. Synthetic oligonucleotides coding for human integrin αIIb TMCD residues E^{960}-E^{1008} and the $R^{995}D$ mutant, and β3 TMCD residues K^{689}-T^{762} and the $I^{704}A$ mutant were amplified by PCR and subcloned into the pMAL-C2 vector (New England Biolabs, Inc.) containing a highly soluble N-terminal fusion maltose-binding protein (MBP). To enhance purification and reduce nonspecific cleavage of target peptide, the original Factor Xa cleavage site between MBP and target peptide was replaced by a hexa-His tag and tobacco etch virus (TEV) cleavage site. Expression was induced in *E. coli* BL21(DE3) cells by adding isopropyl-β-D-thiogalactoside (IPTG) to 1.0 mM. ^{15}N and/or ^{13}C isotope labeling was achieved by employing $^{15}NH_4Cl$ (1.1 g/L) and/or ^{13}C glucose (3 g/L) as the sole nitrogen and carbon sources in the cultures. ^{2}H isotope labeling was achieved by using ^{2}H glucose (3g/L) and preparing the culture in 99.8% D_2O. Cells were harvested by centrifugation 4 h after induction and lysed by freezing in liquid nitrogen and treating with lysozyme (5 mg/L culture), DNase I (0.5 mg/L culture), Complete Protease Inhibitor (0.5 tablet/L culture) in running buffer (50 mM NaH_2PO_4/Na_2HPO_4, 300 mM NaCl, pH 8.0) plus 0.5% Triton X-100 (vol/vol) at 4 °C overnight. The lysate was applied on a 5 mL HisTrap column (GE Healthcare, Inc.) charged with Ni^{2+} for immobilized metal affinity chromatography (IMAC). The column was washed with 10 column volumes of running buffer plus 20 mM imidazole, and the bound protein was eluted by increasing the imidazole concentration from 20 mM to 400 mM linearly in 8 column volumes and collected according to the 280 nm absorbance. The eluent was then buffer exchanged to TEV cleavage buffer (50 mM NaH_2PO_4/Na_2HPO_4, 150 mM NaCl, 0.3 mM Tris(2-carboxyethyl)phosphine hydrochloride (TCEP), 7.5% Glycerol (vol/vol), pH 7.4) via a HiPrep 26/10 desalting column (GE Healthcare, Inc.). The MBP and 6xHis tag were removed from αIIb/β3 TMCD peptides by TEV enzyme, leaving additional GAMGS fragment at the N-terminal of the peptide. The cleaved sample was dialyzed at 4 °C against water for 1 day. The precipitate—αIIb/β3 TMCD peptide—was further purified by reversed-phase HPLC on a Vydac C4 analytical column using a linear gradient from 60%/40% buffer A (H_2O, 0.1% trifluoroacetic acid (TFA), 0.1% hexafluoroisopropanol (HFIP))/buffer B (Acetonitrile, 0.07% TFA, 0.1% HFIP) to 30%/70% in 40 min. Peptide purity/mass were verified by SDS/PAGE and MALDI-TOF mass spectrometry. Our yield was approximately 3 mg/L culture for αIIb TMCD and 1 mg/L culture for β3 TMCD.

NMR Sample Preparation. The following membrane-mimetic solvent media were explored: (*a*) Sodium Dodecyl Sulfate (SDS) micelles; (*b*) n-Dodecyl-PhosphoCholine (DPC) micelles; (*c*) n-Decyl-β-D-Maltopyranoside (DM) micelles; (*d*) n-Octyl-β-D-Glucopyranoside (OG) micelles; (*e*) 1,2-Di-Hexanoyl-sn-glycero-3-PhosphoCholine (DHPC) micelles; (*f*) 1-Palmitoyl-2-Hydroxy-sn-glycero-3-Phophos-rac-(1-Glycerol) (LPPG) micelles; (*g*) DHPC/1,2-Di-Myristoyl-sn-glycero-3-PhosphoCholine (DMPC) bicelles; (*h*) CD_3OH; (*i*) CD_3Cl_3/CD_3OH; (J) CF_3CD_2OD/H_2O; (*k*) CD_3CN/H_2O. All these media are often used to study membrane protein structures (1). Micelle conditions (*a*) and (*b*), but not (*c*–*h*), gave uniform signals in HSQC spectra. However, they failed to reveal αIIbβ3 TMCD interaction as noted previously (2). Bicelles condition (*g*) also failed to reveal significant interaction in our hands, although similar conditions employing truncated constructs (αIIb truncated at P^{998} and β3 truncated at F^{727}) allowed Lau et al. (3) to detect a heterodimer. However, the NMR spectra in Lau et al. (3) indicated the presence of both monomer and dimer, making high resolution spectral analysis rather difficult. Indeed, only 100 intrasubunit NOEs (primarily sequential NH-NH NOEs) and 26 intersubunit NOEs were reported. Among the organic solvent/water conditions (*h*–*k*), we found that K with 50%/50% CD_3CN/H_2O gave excellent NMR spectra and allowed detailed structural characterization of specific interactions between the 2 subunits (Fig. S1).

Organic solvent/water systems have been previously proven useful for studying the structures of transmembrane proteins (1), and were shown to provide native membrane-equivalent structural information (4–14). The advantage of the organic solvent/water mixture systems is that they are isotropic, ideal for high resolution NMR analyses and for examining weak TM interactions. Such mixtures also exhibit partitioning of hydrophobic and hydrophilic phases mimicking the membrane-water interface (1, 15). This is particularly useful for the present case containing both hydrophobic TM and hydrophilic CT.

NMR Spectroscopy. All heteronuclear NMR experiments were performed at 25 °C on Bruker Avance 600 MHz, 800 MHz, and 900 MHz spectrometers equipped with cryogenic triple resonance probes and shielded z-gradient units. The backbone and side-chain ^{1}H, ^{13}C, and ^{15}N resonances were assigned based on triple-resonance NMR spectra of HNCA, HNCO, HNCACB, CBCACONH, H(CCO)NH, and C(CCO)NH (16). NOE distance restraints for structure calculations of the free and bound αIIb and β3 TMCDs were obtained from $^{15}N/^{13}C$-edited 3D NOESY spectra (mixing time 150 ms). Intermolecular NOE distance restraints between αIIb and β3 TMCDs for the complex calculation were obtained from ^{15}N-edited NOESY (17) using either $^{15}N/100\%^{2}H$-labeled αIIb TMCD/unlabeled β3 TMCD or vice versa (mixing times were 200 ms, 300 ms, and 400 ms respectively to eliminate possible spin diffusion effects), and $^{15}N/^{13}C$-edited $^{15}N/^{13}C$-filtered 3D NOESY (mixing time 150 ms) (18). Processing and analysis was done using nmrPipe (19), NMRView (20), PASA (21), and PIPP (22).

Structure Calculations. The structures of the αIIb and β3 TMCD in their free forms were calculated as described in ref. 23. For the heterodimeric αIIbβ3 complex, we first calculated the structures of bound forms of αIIb and β3 TMCDs separately using standard protocols with NOE distance constraints, and backbone φ,ψ-constraints obtained from program TALOS (24). In the next round, a group of unambiguously assigned intermolecular NOEs were incorporated for the complex structure calculation by docking the bound αIIb and β3 TMCD structures. The calculation was performed using Xplor-NIH (25). All structures satisfying the experimental restraints (i.e., both the intramolecular and intermolecular distance restraints and the dihedral angle constraints) converged to a single cluster. In the next iterations, the ambiguity in the intermolecular restraints, especially TM methyls-related intermolecular NOEs, was gradually reduced by examining the resulting structures so that more intermolecular NOEs were assigned. Using randomly oriented starting structures, a total of 98 final structures were calculated and the 20 lowest energy structures were chosen for analysis. A

total of 2018 intrasubunit NOEs, 148 TALOS-based dihedral angle constraints, 213 backbone hydrogen-bond constraints, 82 intermolecular NOEs led to tight convergence of the complex structure (see Table S1 for structural statistics). The hydrogen-bond restraints, primarily for the TM regions, were only incorporated at the final stage of the calculations for the α-helix elements identified from previous rounds of structure calculations. Structure quality was evaluated using the program PROCHECK (26).

1. Henry GD, Sykes BD (1994) Methods to study membrane protein structure in solution. *Methods Enzymol* 239:515–535.
2. Li R, et al. (2001) Oligomerization of the integrin alpha IIbbeta 3: Roles of the transmembrane and cytoplasmic domains. *Proc Natl Acad Sci USA* 98:12462–12467.
3. Lau TL, Kim C, Ginsberg MH, Ulmer TS (2009) The structure of the integrin alphaIIb-beta3 transmembrane complex explains integrin transmembrane signalling. *EMBO J* 28:1351–1361.
4. Wallace BA, Raviknmar K (1988) The gramicidin pore: Crystal structure of a cesium complex. *Science* 241:182–187.
5. Gargaro AR, Bloomberg GB, Dempsey CE, Murray M, Tanner MJ (1994) The solution structures of the first and second transmembrane-spanning segments of band 3. *Eur J Biochem* 221:445–454.
6. Pervushin KV, Orekhov VY, Popov AI, Musina LY, Arseniev AS (1994) Three-dimensional structure of (1–71) bacterioopsin solubilized in methanol/chloroform and SDS micelles determined by 15N–1H heteronuclear NMR spectroscopy. *Eur J Biochem* 219:571.
7. Schwaiger M, et al. (1998) NMR investigation of the multidrug transporter EmrE, an integral membrane protein. *Eur J Biochem* 254:610–619.
8. Dmitriev O, Jones PC, Jiang WP, Fillingame RH (1999) Structure of the Membrane Domain of Subunit *b* of the *Escherichia coli* F_0F_1 ATP Synthase. *J Biol Chem* 274:15598.
9. Rastogi VK, Girvin ME (1999) Structural changes linked to proton translocation by subunit c of the ATP synthase. *Nature* 402:263–268.
10. Engler A, Stangler T, Willbold D (2002) Structure of human immunodeficiency virus type 1 Vpr(34–51) peptide in micelle containing aqueous solution. *Eur J Biochem* 269:3264–3269.
11. Ma D, Liu Z, Li L, Tang P, Xu Y (2005) Structure and dynamics of the second and third transmembrane domains of human glycine receptor. *Biochemistry* 44:8790–8800.
12. Nakano T, Ikegami T, Suzuki T, Yoshida M, Akutsu H (2006) A new solution structure of ATP synthase subunit c from thermophilic Bacillus PS3, suggesting a local conformational change for H+-translocation. *J Mol Biol* 358:132–144.
13. Wang ZY, Gokan K, Kobayashi M, Nozawa T (2005) Solution structures of the core light-harvesting alpha and beta polypeptides from Rhodospirillum rubrum: Implications for the pigment-protein and protein-protein interactions. *J Mol Biol* 347:465–477.
14. Wang ZY, Suzuki H, Kobayashi M, Nozawa T (2007) Solution structure of the Rhodobacter sphaeroides PufX membrane protein: Implications for the quinone exchange and protein-protein interactions. *Biochemistry* 46:3635–3642.
15. Mottamal M, Shen S, Guembe C, Krilov G (2007) Solvation of transmembrane proteins by isotropic membrane mimetics: A molecular dynamics study. *J Phys Chem B* 111:11285–11296.
16. Bax A, Grzesiek S (1993) Methodological advances in protein NMR. *Acc Chem Res* 26:131–138.
17. Walters KJ, Matsuo H, Wagner G (1997) A simple method to distinguish intermonomer nuclear overhauser effects in homodimeric proteins with C_2 symmetry. *J Am Chem Soc* 119:5958–5959.
18. Zwahlen C, et al. (1997) Methods for measurement of intermolecular NOEs by multinuclear NMR spectroscopy: Application to a bacteriophage λ N-peptide/*box*B RNA complex. *J Am Chem Soc* 119:711–721.
19. Delaglio F, et al. (1995) NMRPipe: A multidimensional spectral processing system based on UNIX pipes. *J Biomol NMR* 6:277–293.
20. Johnson BA (2004) Using NMRView to visualize and analyze the NMR spectra of macromolecules. *Methods Mol Biol* 278:313–352.
21. Xu Y, Wang X, Yang J, Vaynberga J, Qin J (2006) PASA—A program for automated protein NMR backbone signal assignment by pattern-filtering approach. *J Biomol NMR* 34:41–56.
22. Garrett DS, Powers R, Gronenborn AM, Clore GM (1991) A common sense approach to peak picking in two- three- and four-dimensional spectra using automatic computer analysis of contour diagrams. *J Magn Reson* 95:214–220.
23. Vinogradova O, et al. (2004) Membrane-mediated structural transitions at the cytoplasmic face during integrin activation. *Proc Natl Acad Sci USA* 101:4094–4099.
24. Cornilescu G, Delaglio F, Bax A (1999) Protein backbone angle restraints from searching a database for chemical shift and sequence homology. *J Biomol NMR* 13:289–302.
25. Schwieters CD, Kuszewski JJ, Tjandra N, Clore GM (2003) The Xplor-NIH NMR molecular structure determination package. *J Magn Reson* 160:65–73.
26. Laskowski RA, MacArthur M, Moss DS, Thornton JM (1993) PROCHECK: A program to check the stereochemical quality of protein structures. *J Appl Crystallogr* 26:283–291.
27. Zhu J, Luo BH, Xiao T, Zhang C, Nishida N, Springer TA (2008) Structure of a complete integrin ectodomain in a physiologic resting state and activation and deactivation by applied forces. *Mol Cell* 32:849–861.
28. Vinogradova O, et al. (2002) A structural mechanism of integrin alpha(IIb)beta(3) ''inside-out'' activation as regulated by its cytoplasmic face. *Cell* 110:587–597.
29. Shen Y, Vernon R, Baker D, Bax A (2009) De novo protein structure generation from incomplete chemical shift assignments. *J Biomol NMR* 43:63–78.

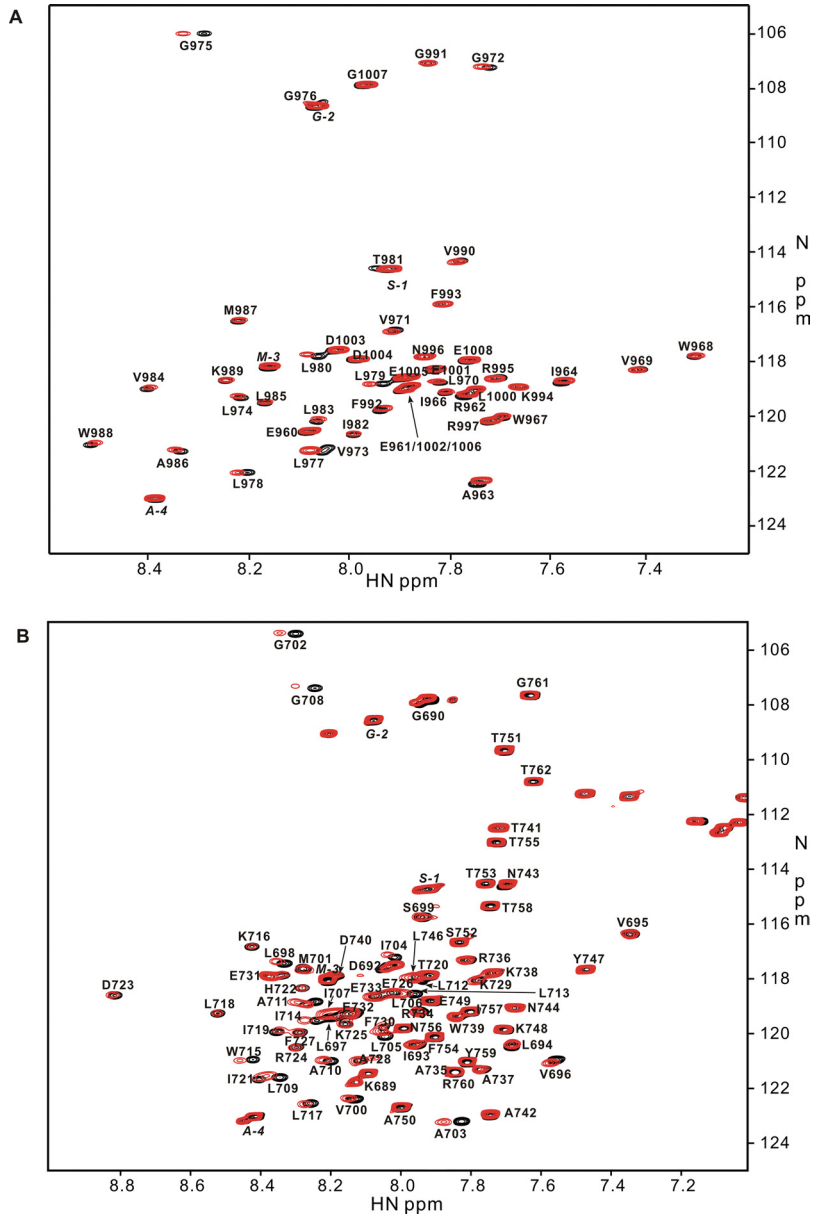

Fig. S1. NMR evidence of integrin αIIbβ3 TMCD interaction. (*A*) 2D ^{1}H-^{15}N HSQC of ^{15}N-labeled 0.1 mM αIIb TMCD in the absence (black) and presence (red) of 0.3 mM unlabeled β3 TMCD in 50%CD_3CN/50%H_2O, 0.1% TFA, 25 °C. Notice the perturbed residues, which involve transmembrane and membrane-proximal regions of αIIb TMCD. Also notice R^{995} that is involved in interacting with β_3 CT D^{723} is also perturbed. Residues labeled with negative signs belong to linker. The small-to-modest chemical shift changes indicate the interaction is relatively weak. (*B*) 2D ^{1}H-^{15}N HSQC of ^{15}N-labeled 0.1 mM β3 TMCD in the absence (black) and presence (red) of 0.3 mM unlabeled αIIb TMCD in 50%CD_3CN/50%H_2O, 0.1% TFA, 25 °C.

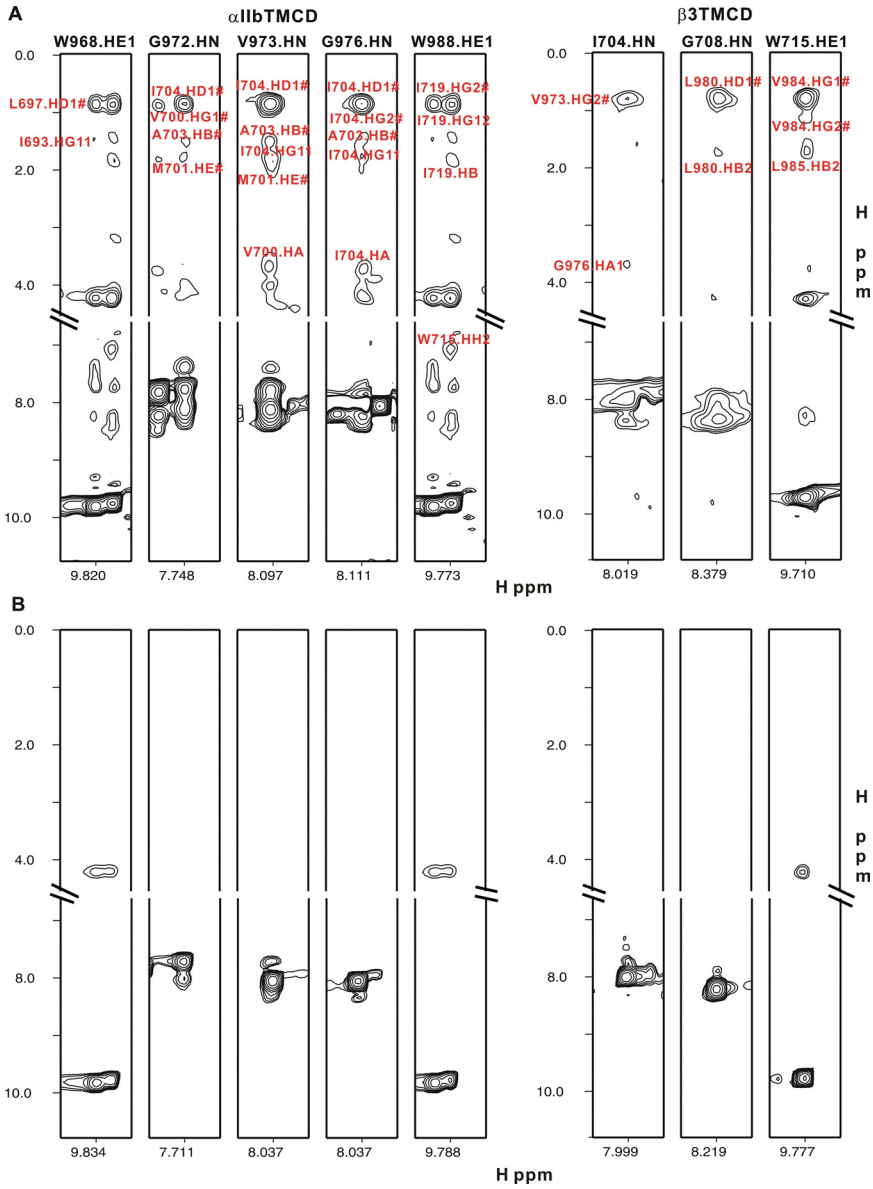

Fig. S2. Intermolecular NOE contacts between αIIb and β3 TMCDs. Selected strips of ^{15}N-edited NOESY spectra of (*A*) ^{15}N/100%^{2}H-labeled αIIb TMCD in the presence of unlabeled β3 TMCD and vice versa. Intermolecular NOE assignments are labeled in red; Note that peaks at approximately 4.2 ppm in some strips arise from water. Numerous nonmethyl peaks can be assigned unambiguously. Some degenerate methyl-related peaks were assigned to more than one contact only during the later stage of the structure refinement. (*B*) Control data with ^{15}N/100%^{2}H-labeled αIIb TMCD in the absence of unlabeled β3 TMCD or vice versa, showing no intermolecular NOEs.

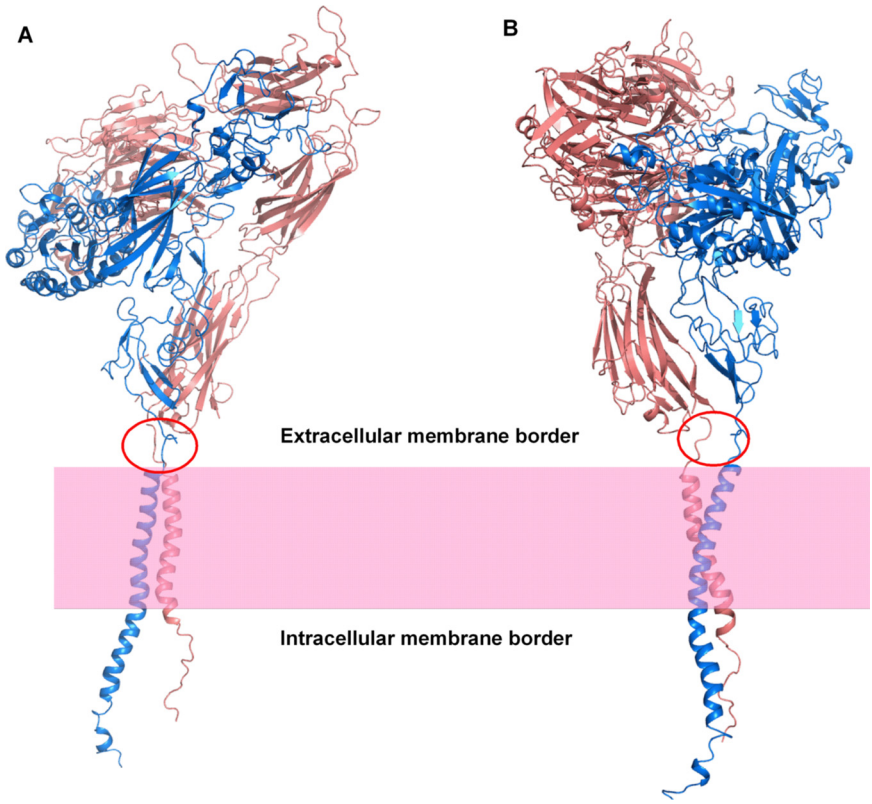

Fig. S3. Two different views of the αIIbβ3 TMCD complex structure fused to the complete ectodomain (27). Notice that the C-termini of the ectodomain are very close to the extracellular membrane border via short loops shown in our structure (red circles).

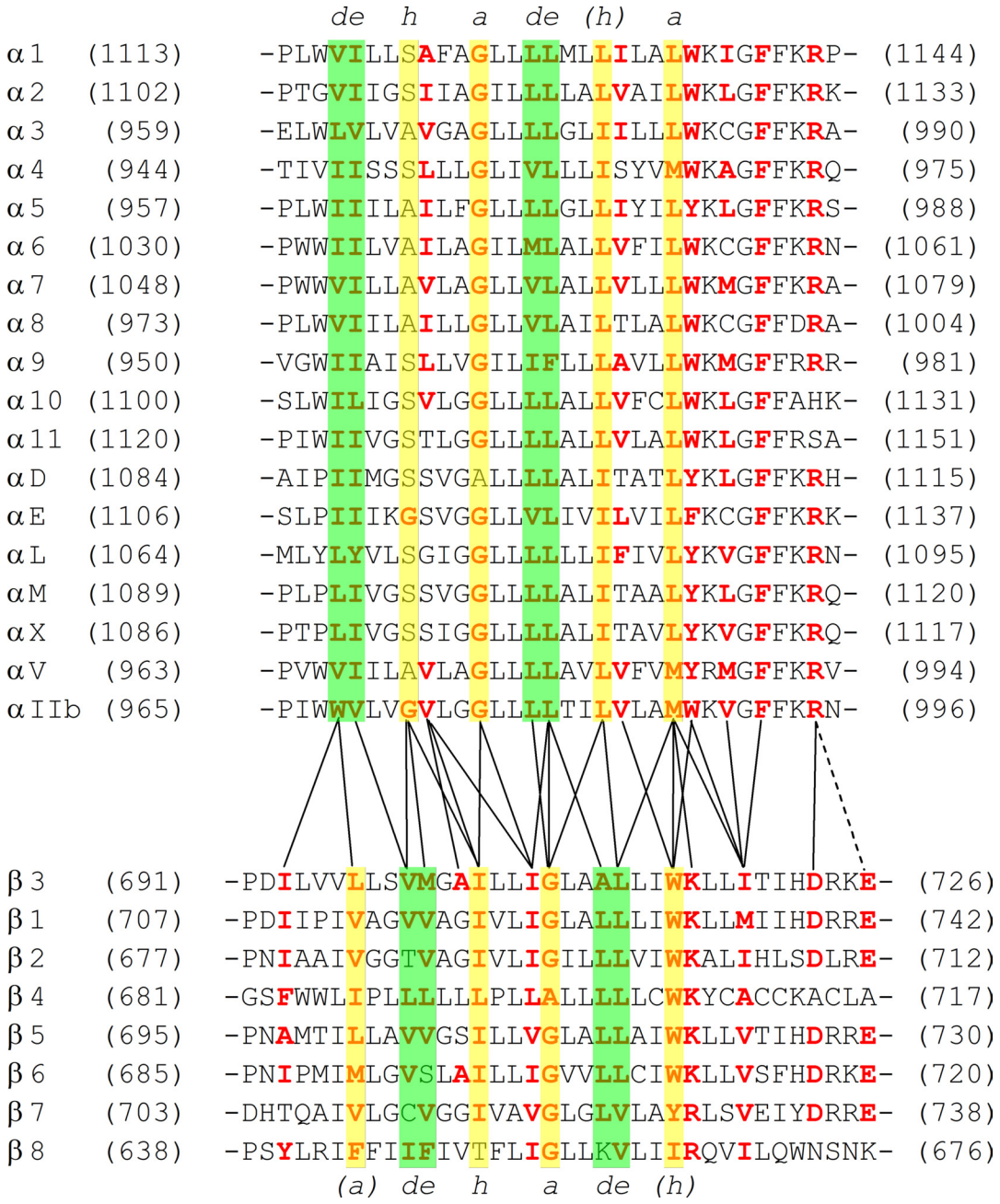

Fig. S4. Sequence alignment of αIIb/β3 TMCD interface residues with other integrins. Highly conserved residues that are involved in the interface are highlighted in αIIbβ3 and all other integrins. Potential coiled-coil residues in other integrins are shaded as compared to those in αIIbβ3. Residue-based interaction networks (based on ^{1}H-^{1}H distances <5 Å) are drawn between αIIb and β3 TMCDs using solid lines. A dotted line between αIIb R^{995} and β3 E^{726}, indicates a potential salt-bridge that is less well defined in the ensemble structures as compared to αIIb R^{995}/β3 D^{723} salt bridge.

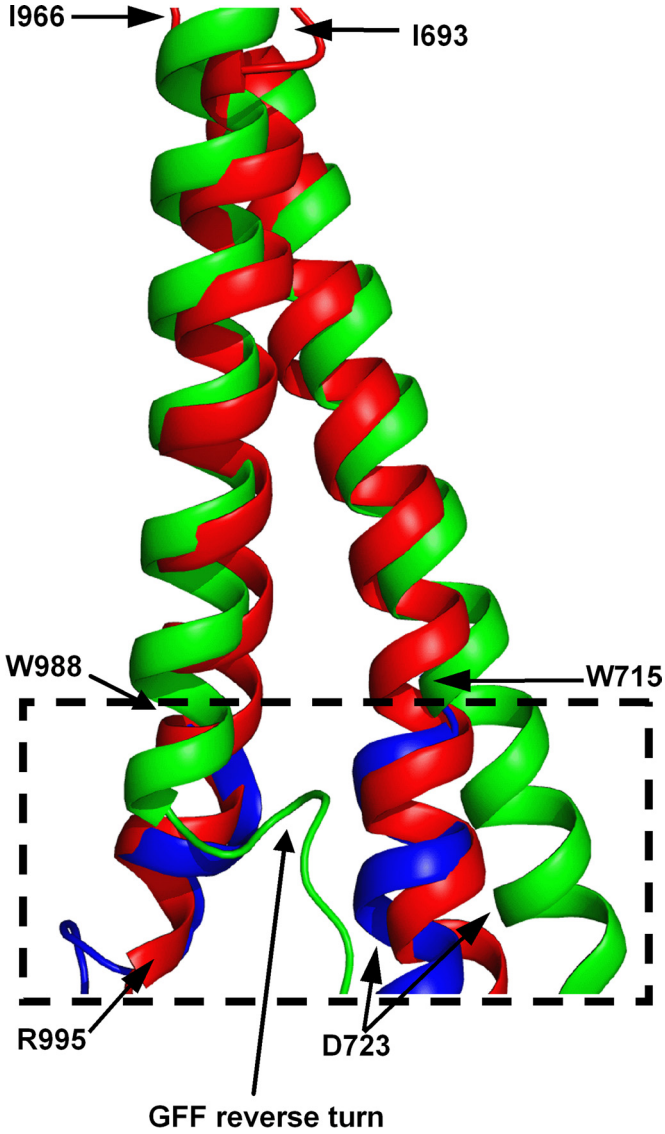

Fig. S5. Structural comparison of αIIbβ3 TMCD complex in CD_3CN/H_2O (red) with that in bicelles (green) (3) (the overlay was made between αIIb I693-W988/β3 I966-W715 with the backbone rmsd of 2.06 Å). The rectangle (dotted line) highlights the comparison of the membrane-proximal clasps by 3 studies: (*i*) the αIIbβ3 TMCD complex in CD_3CN/H_2O (red); (*ii*) the CT complex in aqueous solution (28) (blue); (*iii*) the αIIbβ3 TMCD complex in bicelles (green). The overall topologies of the clasps in (*i*) and (*ii*) are very similar (the overlay was made between αIIb K989-R995 and β3 K716-D723), but they are different from that in bicelles primarily due to the GFF reverse turn.

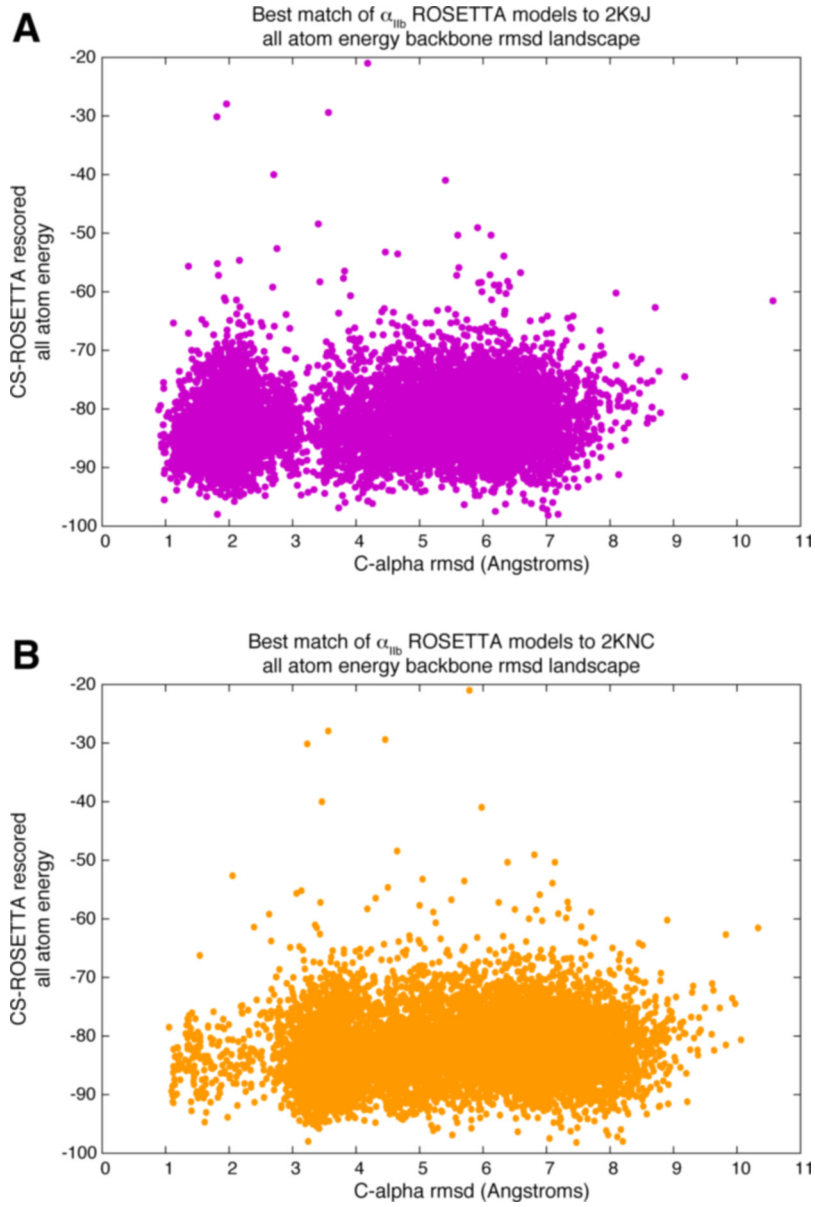

Fig. S6. 10229 αIIb models were generated by CS-ROSETTA (29) using experimental chemical shifts assigned in a CD_3CN/H_2O solvent system as an input during fragment selection. Convergence plots of CS-ROSETTA rescored all atom energies versus the backbone rmsd between each generated αIIb model and the αIIb chain of search model 2K9J (3) (*A*) (magenta) and our model 2KNC (*B*) (orange) All 10229 αIIb models were rescored using CS-ROSETTA by incorporating ROSETTA all atom energy scores with a rescoring term calculated by comparing predicted backbone chemical shifts for each αIIb model to the experimental chemical shifts for αIIb (960–1008) assigned in a CD_3CN/H_2O solvent system. Backbone rmsds were calculated with an in-house script using NH, Cα and C′ atoms. 3767 of the 10229 αIIb models aligned to the search model 2K9J with a backbone rmsd $<$3.0 Å. 336 of the 10229 αIIb models aligned to the search model 2KNC with a backbone rmsd $<$3.0 Å.

Table S1. Structural statistics of the αIIbβ3 TMCD heterodimer

		αIIb/β3 TMCD Complex
Number NOEs		
	All	2100
	Sequential, i-j =1	664
	Medium range, 1< i-j <5	688
	Long range, i-j ≥5 (82 intermolecular NOEs)	83
	Hydrogen-bond	213[a]
Rmsd from experimental distance restraints (Å)[b]		
	All	0.073 ± 0.003
	Sequential, i-j =1	0.057 ± 0.001
	Medium range, 1< i-j <5	0.048 ± 0.001
	Long range, i-j ≥5	0.058 ± 0.004
Rmsd from experimental dihedral restraints (°)		
		0.748 ± 0.092
Rmsd from idealized covalent geometry		
	Bonds (Å)	0.0070 ± 0.0001
	Angles (°)	0.895 ± 0.011
	Impropers (°)	2.145 ± 0.003
E_{L-J} (kcal/mol, based on CHARMM19 parameters)		
		−381.5 ± 10.3
Ramachandran plot		
	Most favored regions (%)	73.4
	Additionally and generously allowed regions (%)	25.8
	Disallowed regions (%)	0.8
Coordinate precision (Å)		
Structured regions (αIIb 966–996 and β3 693–740)	Backbone atoms	1.08 ± 0.25
	All heavy atoms	1.47 ± 0.29
TMCD interface (αIIb 966–995 and β3 693–723)	Backbone atoms	0.60 ± 0.16
	All heavy atoms	0.90 ± 0.13

[a]Backbone hydrogen-bond constraints, primarily for the TM regions, were only incorporated during final step of calculations based on the α-helix elements identified from the previous rounds of calculations.
[b]Mean ± standard deviation over 20 structures with lowest energies.

Table S2. Functional/structural relationships of single TMCD mutations in αIIbβ3[a]

TMCD mutations	Result	Possible structural consequences	References
αIIb $G^{972}L$, $G^{976}L/I$ $\beta3$ $G^{708}L/I$	++	Strong steric interface clash	1, 2
αIIb $L^{980}A$, $L^{983}A$ $\beta3$ $I^{704}A$, $I^{719}A$ or $I^{719}M$	+	Core interface mutations disrupt interface. $I^{719}M$ swaps between $\beta3$ and $\beta1$, indicating the high specificity of this position in mediating the TMCD heterodimerization.	1–3
αIIb $T^{981}L/I$	+	Partial activation probably due to the destabilization of the αIIb TM helix by disrupting potential H-bonds of T^{981} side chain OH with both carbonyls of αIIb L^{977}/L^{978}.	1, 4
αIIb $F^{992}A$, $F^{993}A$	+	Impairing interface ($F^{992}A$),W^{988}/F^{992} stacking for helix stability, and membrane anchoring (both F^{992} and F^{993}). The mutations may also disrupt the binding to other cytoplasmic regulators.	5
αIIb $R^{995}A/D/Q$ $\beta3$ $D^{723}A/H$	+	Disrupting interface salt-bridge. $R^{995}Q$ induces Glanzmann's thrombasthenia syndrome. $D^{723}H$ causes thrombocytopenia.	5–8
αIIb $I^{966}L$, $W^{967}L$, $V^{971}L$, $V^{973}L$, $G^{975}L$, $I^{982}L$, $A^{986}L$ $\beta3$ $V^{695}L$, $S^{699}L$, $G^{702}L$, $I^{707}L$, $A^{710}L$, $I^{714}L$, $T^{720}I$	−	Non-interface mutations	1, 3
αIIb $W^{968}L$, $V^{969}L$, $V^{984}L$, $M^{987}L$, $W^{988}L$ $\beta3$ $V^{700}L$, $M^{701}L$, $A^{703}L$, $A^{711}L$, $W^{715}L$	−	Interface edge mutations (e.g., $\beta3$ $A^{703}L$, $A^{711}L$) or interface mutations with similar sizes (e.g., $\beta3$ $M^{701}L$) may lead to minor adjustment of the interface packing. Note that while $\beta3$ $V^{700}L$ had little effect, the corresponding $\beta2$ mutation of $T^{686}V/S/F$ activates $\alpha L\beta2$	1, 9

[a]For TM region, only hydrophobic mutations were considered here. − indicates little or negligible activation; + indicates medium or partial activation, and ++ indicates very strong activation.

1. Luo BH, Carman CV, Takagi J, Springer TA (2005) Disrupting integrin transmembrane domain heterodimerization increases ligand binding affinity, not valency or clustering. *Proc Natl Acad Sci USA* 102:3679–3684.
2. Li W, et al. (2005) A push-pull mechanism for regulating integrin function. *Proc Natl Acad Sci USA* 102:1424–1429.
3. Hato T, et al. (2008) Cooperative role of the membrane-proximal and -distal residues of the integrin beta3 cytoplasmic domain in regulation of talin-mediated alpha IIb beta3 activation. *J Biol Chem* 283:5662–5668.
4. Partridge AW, Liu S, Kim S, Bowie JU, Ginsberg MH (2005) Transmembrane domain helix packing stabilizes integrin alphaIIbbeta3 in the low affinity state. *J Biol Chem* 280:7294–7300.
5. Hughes PE, et al. (1996) Breaking the integrin hinge: a defined structural constraint regulates integrin signaling. *J Biol Chem* 271:6571–6574.
6. Ma YQ, et al. (2006) Regulation of integrin αIIb$\beta3$ activation by distinct regions of its cytoplasmic tails. *Biochemistry* 45:6656–6662.
7. Ghevaert C, et al. (2008) A nonsynonymous SNP in the ITGB3 gene disrupts the conserved membrane-proximal cytoplasmic salt bridge in the αIIb$\beta3$ integrin and cosegregates dominantly with abnormal proplatelet formation and macrothrombocytopenia. *Blood* 111:3407–3414.
8. Peyruchaud O, et al. (1998) R to Q amino acid substitution in the GFFKR sequence of the cytoplasmic domain of the integrin IIb subunit in a patient with a Glanzmann's thrombasthenia-like syndrome. *Blood* 92:4178–4187.
9. Vararattanavech A, Lin X, Torres J, Tan SM (2009) Disruption of the integrin alphaLbeta2 transmembrane domains interface by beta2 Thr686 mutation activates alphaLbeta2 and promotes micro-clustering of the alphaL subunits. *J Biol Chem* 284:3239–3249.